Published by :
http://www.ijert.org

International Journal of Engineering Research & Technology (IJERT)
ISSN: 2278-0181
Vol. 5 Issue 08, August-2016

# Simulation of Dust Pre-Separation in Axial Entry Gas Cyclone using CFD

Ravichandran Srinivasan[†]
[†] CORI
(Crucible of Research and Innovation),
PES University, Bengaluru, India

Suresh Nagesh[ǂ]
[ǂ] CORI
(Crucible of Research and Innovation),
PES UniversityBengaluru, India

Chetan B M[‡]
[‡] CORI
(Crucible of Research and Innovation),
PES University, Bengaluru, India

Martin J. Lehmann*
*Mann+Hummel
Gmbh, Ludwigsburg,
Germany

Volker Greif**
**Mann+Hummel
Gmbh, Speyer,
Germany

Kumar Ramaiah[¶]
[¶]Mann+Hummel Service Center
Bengaluru, India

Antomon Chowallur[§]
[§]Mann+Hummel Service Center,
Bengaluru, India

Srikanth S. R[§§]
[§§]Mann+Hummel Service Center,
Bengaluru, India

Ashish S[Ψ]
[Ψ]Mann+Hummel Service Center,
Bengaluru, India

***Abstract*—Gas cyclones are the devices used to separate discrete phase (dust) from continuous phase (air). In the current study, a Computational Fluid Dynamics (CFD) methodology based on flow simulation combined with Lagrangian particle tracking has been used to calculate pressure drop and pre-separation efficiency for a single cyclone element of axial entry type. This work tries to quantify the effects of flow rate, particle size and its distribution on pressure drop across the cyclone and separation efficiency. In particular the discrete phase method (DPM) has been investigated extensively for particle wall interactions for the relevant range of tangential and normal restitution coefficients. The study shows that good correlation with experimental data for separation efficiency may be realized by an optimal choice of these coefficients.**

***Keywords*—Computational fluid dynamics (CFD), axial entry cyclones, DPM, wall collision.***

## I. NOMENCLATURE

| | |
|---|---|
| $c_p$ | specific heat capacity (J/kgK) |
| ρ | density (kg/m$^3$) |
| $y^+$ | non-dimensional distance from the wall |
| D | diameter of cyclone (mm) |
| d | diameter of dust particles (µm) |
| $C_D$ | Drag Coefficient |
| $\delta_{ij}$ | kronecker delta |
| $u$ | Instantaneous velocity component (m/s) |
| $\bar{u}$ | mean velocity component (m/s) |
| $u'$ | fluctuating velocity component (m/s) |
| p | pressure static (Pa) |
| $P_d$ | dynamic pressure at the inlet (Pa). |
| ΔP | static pressure drop (Pa) |
| NPSE | Normalized pre-separation efficiency |

## I. INTRODUCTION

Cyclone separation is a process of removing suspended particles from air, gas or liquid streams by inducing a vortex. The vortex causes high density particles in the continuous phase to separate due to the difference in inertia. These particles are then removed from the cyclone through a scavenging exit. The manner in which the swirl is induced depends on the geometry of the cyclone used. In case of tangential entry, the swirl is induced because of the cylindrical body and in case of axial entry, vanes are provided at an angle to the flow stream to induce swirl. The swirling action of the flow causes the dust particles to migrate radially towards the walls because of the higher inertia, thus separating out from the main flow.

The cyclone used for the purpose of investigation in the present work is an axial entry cyclone. Generally, in a cyclone separator multiple cyclone elements are used in a particular arrangement to enhance the dust separation efficiency. Partially filtered air from the cyclone separator is then passed through a filter element to remove remaining finer dust particles before entering downstream systems. Marinuc et al. [1] carried out theoretical investigations to determine the variation in the separation efficiency of a tangential cyclone with respect to input velocities, particle diameters and input cross sectional areas using an empirical model proposed by Leith and Litch (1972). It was found that the highest efficiency was achieved for a particular inlet cross sectional area. Separation efficiency was close to 100% for sizes above 400 µm and also it was reported that higher input velocities coupled with smaller inlet areas resulted in higher separation efficiency. Faulkner et al. [2]quantify the effect of inlet velocity on maximum collection efficiency based on two particular models of tangential cyclone (2D2D and 1D3D) and also the pressure drop associated with them. Alumina and corn starch were used as discrete phase. It was found that input velocity for mass loading rates below 2 g/m$^3$ did not significantly affect the separation efficiency when corn starch was used compared to that of alumina. Sakura et al. [3] report the collection efficiencies for a cylindrical inlet

International Journal of Engineering Research & Technology (IJERT)
ISSN: 2278-0181
Vol. 5 Issue 08, August-2016

type cyclone separator at different mass loading conditions and inlet velocities. It was found that the Smolik empirical method [4], [5] under predicts the cyclone efficiency for higher mass loading whereas it agreed well with experimental data for small mass loading rates. Similar results were found with Muschelknautz model [6], [7].Gimbun et al. [8]present the CFD calculation to predict and evaluate the effects of inlet velocity, operating pressure and temperature on the dust separation efficiency of tangential gas cyclones. The RSM turbulence model was used for the computation. It was found that the CFD simulation predicted the collection efficiencies with an error of 3.7% from the measured data. José de Souza et al. [9]investigated particle gas flow in a cyclone using large eddy simulation (LES). It was found that with increase in the gas flow rate, separation efficiency increases. This is mainly due to the increased centrifugal force, which contributes to separation as opposed to turbulence. It was also found that the largest discrepancies between the experiment and simulation occur at midsized particles. Shalabyet et al. [10] investigated the pressure drop, particle trajectories and cyclone separation efficiency using LES model. The coefficient of restitution (COR) was set to 0.8 (COR is the measure of kinetic energy retained by the particle after collision with wall). The pressure drop was reported to deviate from experimental value by 2%. Sommerfield [11]investigated the effects of particle-wall interaction and inter particle collision on the behavior of solid particles inside a horizontal channel. It was found that the wall collision mean free path decreased with increase in particle size. This also reveals that the larger particles are greatly affected by gravity and saltating motion is found without contacting the upper wall.

## II. MATHEMATICAL MODEL

### A. For Continuous Phase:

The three conservation laws, namely those for mass, momentum and energy form the basis of equations governing the fluid flow. For isothermal compressible flow, Reynolds Averaged Navier Stokes equation (RANS) is

$$\frac{\partial \rho}{\partial t} + \frac{\partial}{\partial x_i}(\rho u_i) = 0 \qquad [1]$$

$$\frac{\partial}{\partial t}(\rho u_i) + \frac{\partial}{\partial x_j}(\rho u_i u_j) = -\frac{\partial p}{\partial x_i} + \frac{\partial}{\partial x_j}\left[\mu\left(\frac{\partial u_i}{\partial x_j} + \frac{\partial u_j}{\partial x_i} - \frac{2}{3}\delta_{ij}\frac{\partial u_i}{\partial x_i}\right)\right] + \frac{\partial}{\partial x_j}\left(-\rho\overline{u_i' u_j'}\right) \quad [2]$$

where $\rho$ is the density of the fluid, μ is viscosity, $u_i$ is i-th mean velocity component and $p$ is mean pressure. The last term on the right in eq.[2] represents the effects of turbulence and needs to be modeled. The standard k-ε turbulence model with standard wall functions is used in the current study with attention paid to near wall mesh spacing that is consistent with the use of wall functions.

### B. For Dispersed Phase:

Trajectories of dust particles dispersed in continuous phase is predicted by integrating the force balance acting on the particle. This balance of forces is given by

$$\frac{d\overline{u_p}}{dt} = F_d\left(\bar{u} - \overline{u_p}\right) + \frac{\bar{g}(\rho_p - \rho)}{\rho_p} + \bar{F} \qquad [3]$$

where the over bar denotes a vector quantity and $\bar{u}$ denotes fluid phase velocity, $\overline{u_p}$ the particle velocity, $F_D(\bar{u} - \overline{u_p})$ is drag force per unit particle mass.

$$F_D = \frac{18\mu}{\rho_p d_p^2}\frac{C_D Re}{24} \qquad [4]$$

$d_p$ is particle diameter, $\rho_p$ is particle density, $Re$ is relative Reynolds number, $\bar{g}$ denotes acceleration due to gravity, $C_D$ is coefficient of drag and $\bar{F}$ involves additional forces like shear and pressure, virtual mass, buoyancy, Basset, lift, Brownian, turbulent dispersion, erosion for harsh environments, surface roughness, and forces due to interaction between particles. In the present study only drag and gravity forces have been included in the simulation. Note that the sign of the drag force depends on that of the relative velocity between that of fluid and the particle. From [4] it can be seen that for the same relative velocity drag force varies inversely as the size of the particle. Therefore in regions where the drag force is negligible due to the relative velocity being small, gravity may dominate the behavior of larger particles as compared to the smaller ones and the choice of wall reflection coefficients may have differential impact on the corresponding separation efficiency

## III. CYCLONE GEOMETRY AND MESH GENERATION

### A. Cyclone Geometry

The axial entry cyclone geometry has a dimension of 64 mm diameter. The experimental setup shown in Figure 1 principally consists of the cyclone element placed in a primary air duct upstream of a scavenging secondary pipe meant for collecting separated dust particles. From the CAD model of the set up that was available, only the wetted surfaces of the air flow were considered for the geometric cleanup and modifications. All the geometric details and the standards of the experimental set up were captured to the best possible extent. This involved extending the CFD domain of the model by six times the respective diameters on all sides. This helped in simulating experimental conditions better to later on validate the numerical results with experimental data.

Further the upstream extension allows the flow to develop before it enters the cyclone.

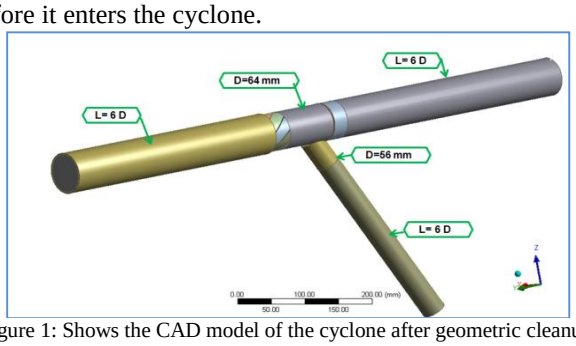


Figure 1: Shows the CAD model of the cyclone after geometric cleanup and domain extension

International Journal of Engineering Research & Technology (IJERT)
ISSN: 2278-0181
Vol. 5 Issue 08, August-2016

*B. Mesh Generation*

A hybrid mesh consisting of hexahedral, tetrahedral and pyramid elements was generated. This approach was taken because it allowed for effective control of element count without having to compromise on the mesh density in regions where high turbulence was suspected. Figures 2 and 3, show views of the mesh at various locations. The boundary layer consisted of 5 hexahedral layers, with the first cell height of 0.1 mm. This resulted in a local $Y^+$ value of around 15 to 40 consistent with the use of standard wall function.

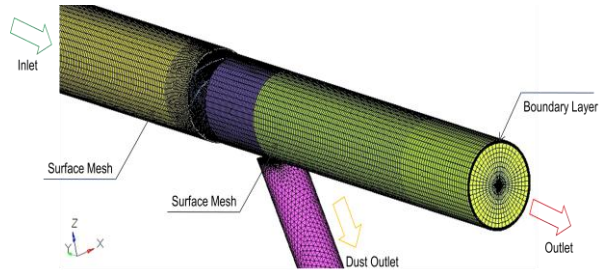


Figure 2: View of the Surface Mesh on Cyclone

The generated mesh was checked for quality, including Jacobian (> 0.6), skewness (< 0.80) and tetcollapse (> 0.4). Mesh convergence study was done for three different mesh sizes 0.5, 1 and 1.7 Million only for flow calculations. It was

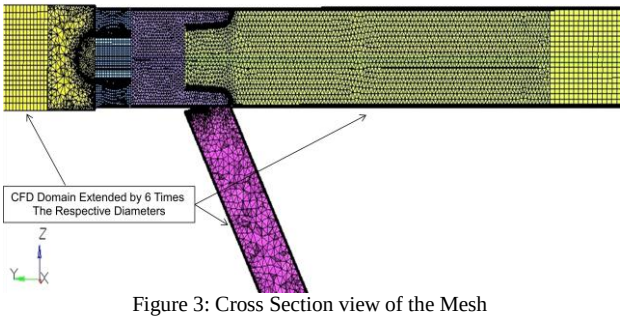


Figure 3: Cross Section view of the Mesh

found that pressure drop for all three meshes were found to be within 4% margin. It was decided to consider 0.5 million cell mesh for all simulations to facilitate subsequent studies with multi-cyclone configurations. Outcome of mesh convergence study are included in results section.

## IV. SOLVER SETUP AND BOUNDARY CONDITIONS

*A. Boundary Conditions for Flow Simulations*

The solver used for setting up and running the simulation was Fluent V15. The turbulence model of choice was the k-ε, with standard wall function and flow is incompressible under current conditions. Since Lagrangian particle tracking calculations were to be carried out later on, gravity was kept on in the direction of the scavenging pipe. Particle interaction effects on fluid flow for the present mass loadings were verified to be negligible. This permitted Lagrangian particle tracking to be decoupled from the flow calculations. Steady state simulation using the SIMPLE pressure-velocity formulation and the coupled solver was used to establish the flow field for different air flow rates. Mass flow is specified at the inlet, and zero gauge pressure condition was set at the main outlet of the cyclone.

Table 1: Problem Set-Up for Flow (With 10% Scavenging)

| | | |
|---|---|---|
| Turbulence Model | K-ε, Standard Wall Function | |
| Gravity | On (Direction of Scavenging Flow) | |
| Boundary Conditions | Inlet | Volume Flow ($m^3$/min) |
| | | 0.86, 1.70, 2.56, 3.42, 4.20 |
| | Dust Outlet | Pressure Outlet With Target Volume Flow ($m^3$/min) |
| | | 0.07, 0.06, 0.18, 0.28, 0.36 |
| | Air Outlet | 0 Gauge Pressure Outlet |
| Pressure-Velocity Coupling Scheme | Coupled | |

*B. DPM Boundary Conditions*

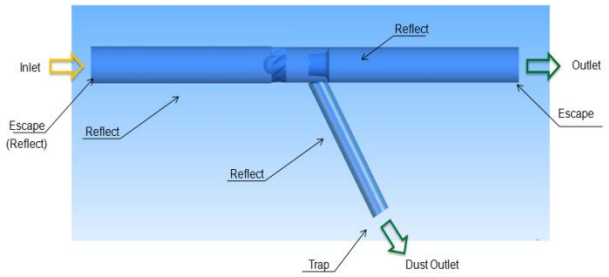


Figure 4: DPM Boundary Conditions

Also in order to maintain approximately 10% of flow through the scavenging pipe a target mass flow condition was set at the dust outlet. Table 1 gives the details and overview of the problem setup.

The boundary conditions for the particle trajectory calculations are shown in Figure 4. While all the conditions indicated are self-explanatory, at the inlet it was found that the escape boundary condition allows many of the particles to reverse their path and escape through the inlet. In an attempt prevent such escapes, the reflect boundary condition is used at the inlet instead.The pre-separation efficiency is defined as

$$Preseparation\ Efficiency = \frac{Particles\ Trapped}{Tracked - Incomplete}$$

where,

*Particles Trapped*—Number of particles leaving domain through scavenging pipe .

*Tracked*— Number of particles injected.

*Incomplete*—Particles whose trajectory calculations are terminated when the maximum number of steps allowed are exceeded.

As the exact location of the particles where the trajectory calculations are terminated is unknown it is better to keep the number of incomplete particles as low as possible by increasing the limit for number of steps. The procedure for particle tracking is as follows.

International Journal of Engineering Research & Technology (IJERT)
ISSN: 2278-0181
Vol. 5 Issue 08, August-2016

Once the flow field is converged the flow equations are turned off and dust particles are injected into the domain at the inlet

Table 2: Solver setup and point properties

| | |
|---|---|
| Paricle Diameter | 1 2,3,4,5,7 ,10,20,40,80,120,180 and 200 and Rosin Rammler Distribution. |
| Particle Density | 2650 kg/m$^3$ |
| Injection Velocity | Inlet air velocity |
| Injection Type | Surface (Inlet) |
| Number of Particles injected | 306 in case of homogeneous injection, 3060 in case of RR Distribution |
| Particle Feed Rate | 1 g/m$^3$ |
| Particle Type | Spherical |
| Tracking Parameters | No. of Steps: 500000<br>Step Length Factor: 5 |
| Coupling | One Way |

surface. Particle inlet velocity is assumed to be same as that of inlet air velocity. Separation efficiencies for individual particles and Rosin-Rammler distribution (see Table 2) are calculated using DPM assuming elastic collision with the walls with default normal and tangential reflection coefficients (1,1) respectively. The effect of the choice of reflection coeficients on separation efficiency of each particle is studied later. Tables 2 and 3 show the solver setup and input parameters for the RR curve approach.

Table 3: Input parameters for RR Curve fit approach

| | |
|---|---|
| Min Diameter (mm) | 0.001 |
| Max Diameter (mm) | 0.2 |
| Mean Diameter (mm) | 0.048 |
| Spread Factor Average (n) | 1.116 |
| No. of Diameters | 10 |

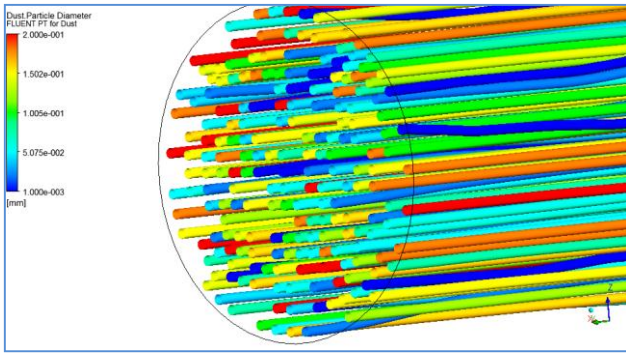


Figure 5: Tracks of particles injected from the inlet face colored by particle diameter

ISO 12103-1standard size distribution has a range of particle sizes between 1 and 200 µm.

In order to incorporate this data into the solver Rosin Rammler curve fit is used. The Rosin-Rammler distribution function ($Y_d$) is given by

$$Y_d = e^{(\frac{d}{\bar{d}})^n} \qquad [5]$$

Where d is diameter, $\bar{d}$ is size constant and n is size distribution parameter.

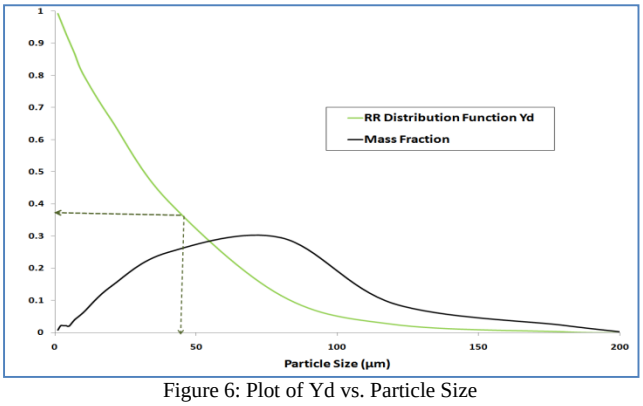


Figure 6: Plot of Yd vs. Particle Size

Figure 6. illustrates the mass fractions of particles of different sizes in ISO 12103-1standard distribution which is used in the current study. The vertical broken line in Figure 6 indicates the average size of particle in the distribution. Figure 7 shows the tracks of 200 out of 3060 particles injected into cyclone from inlet face using RR function.

## V. RESULTS AND DISCUSSIONS

### *A. Flow Simulations and Pressure Drop Calculations.*

The flow results were analyzed in terms of pressure drop (both static and total) across the cyclone for the specified flow rates. The key regions of importance inside the cyclone i.e., behind the vanes and at the interface of the scavenging pipe with the main flow were looked at critically, as it may influence overall performance including separation efficiency. The static pressure is measured in the experimental procedure at specified locations on the cyclone using pressure taps.

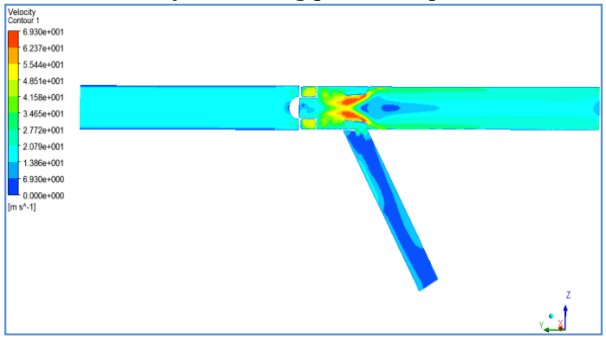


Figure 7: Velocity Contour on the Centre Plane

Figure 7 shows the velocity contours on the mid-plane for a flow rate of 3.11 m$^3$/min. From the figure it is seen that a stagnation point is formed on the upstream dome, around which the flow enters the cyclone through the annulus upstream of the vanes. The turning angle of the vanes induces a tangential component to the incoming air, resulting in a strong vortex structure forming midway through the cyclone. This swirling action causes the air to enter the scavenging pipe, forming a wall jet right at the entry to the scavenging duct. The swirling flow continues a short distance downstream, until it reaches the dip tube entrance, after which it slowly expands into the tapering duct and decays. The fraction of flow entering the scavenging duct is small resulting in the significantly low velocities. In the primary duct there is a strong re-circulation zone, which later straightens along the length of

International Journal of Engineering Research & Technology (IJERT)
ISSN: 2278-0181
Vol. 5 Issue 08, August-2016

the pipe. The primary flow mixes and becomes almost uniform with small transverse gradient, before it reaches the main air outlet.

The variation of calculated static pressure drop normalized by the inlet dynamic head for the three different mesh counts is shown in Table 4. Two planes are created, one at a distance of 2 times the diameter upstream of the cyclone and the other at a distance of 4 times the diameter downstream of the flow. Pressure drop is measured between these two planes.

Table 4: Static Pressure Drops Normalized by dynamic head for 5 Flow Rates Compared with Experimental Values

| Flow Rate ($m^3$/min) | Flow Resistance ($\Delta P/P_d$) With 10% Scavenging | | | |
|---|---|---|---|---|
| | 0.5 Million | 1 Million | 1.7 Million(Polyhedral) | Exp. |
| 0.79 | 8.91 | 8.83 | 9.21 | 7.68 |
| **1.55** | **9.48** | **9.28** | **9.54** | **8.77** |
| 2.33 | 9.30 | 9.10 | 9.41 | 8.03 |
| **3.11** | **9.27** | **9.05** | **9.36** | **7.97** |
| 3.82 | 9.28 | 9.07 | 9.33 | 8.20 |

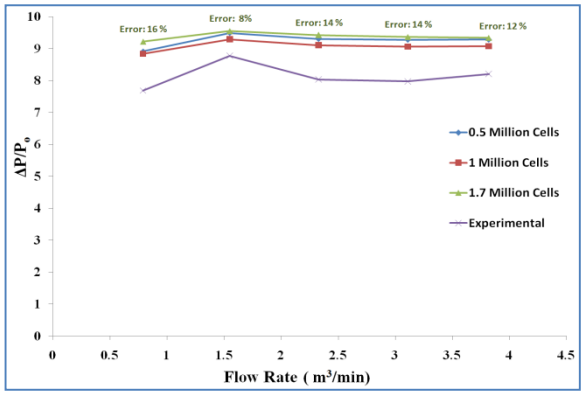


Figure 8: Normalized pressure drop Vs. Flow Rate for 3 Different Mesh Compared with Experimental Data

Figure 8 shows a 8-16% discrepancy between measured and computed values for the range of flow rates calculated. The computed results also show that mesh refinement in the above range has very little effect on the computed pressure drops. Hence for all simulations and for reasons already stated, the 0.5 million cell mesh has been used. Then particles with *ISO* 12103-1 standard size distribution (Rosin-Rammler) are injected to obtain the pre-separation efficiency.

*B. Pre-Separation Efficiency Without Considering Wall Collision Effects.*

*1. Homogeneous Particle Injection*

In an attempt to understand the effect of particle size on separation efficiency under different air flow rate conditions, particle trajectory calculations are carried out for homogeneous particle injection in the range of 1 µm to 200 µm. Separation efficiencies for five different flow rates (1.55, 3.11, 4.6 $m^3$/min) with dust flow rate of 1 g/$m^3$ have been investigated with suction employed at the scavenging dust outlet. All these calculations are done keeping the default wall reflection coefficients i.e (normal, tangential) as (1, 1).

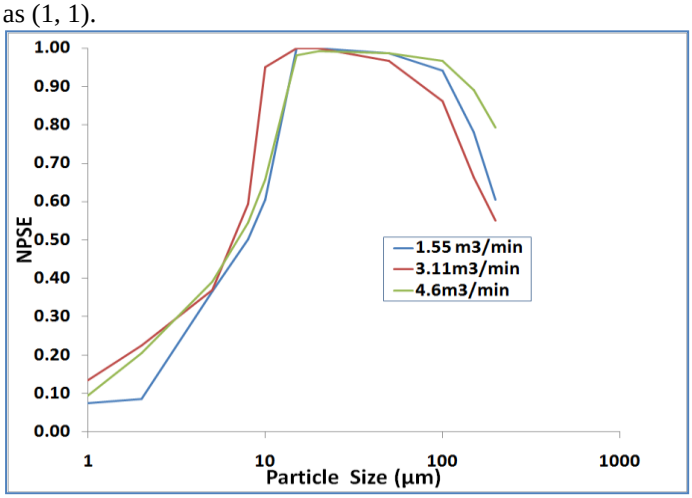


Figure 9: Plots of Normalized Separation Efficiency (%) Vs. Particle Size (µm) for 5 different flow rates [With Scavenging]

Figure 9 summarizes the calculated results for the range of particle sizes considered with forced scavenging for 3 different flow rates.A careful consideration of the plots appears to indicate that the separation efficiency behaves differently for smaller particles as compared to large particles. For paticle size less than about 7µm, flow rate has a favorable effect on separation efficiency whearas for particle size above 100µm, the reverse is the case. For intermediate particle sizes the behavior is somewhat mixed. The sharp decrease in separation efficiency for particle size greater than 100 µmwas not considered reasonable and prompted further investigation. Hence the procedure was repeated with modified wall reflection coefficients of (normal,tangential)-(0.8,0.9). Results plotted in Figure 8 show that appropriate behavior of separation efficiency for larger particle sizes may be realized by a proper choice of wall reflection coefficients. Procedure for selction of reflection coefficients is included in later sections after extensive calculations.

Increase in separation efficieny with particle diameter can be explained by the particle tracks shown in Figure 9,These figures illustrate particle tracks for 1, 5,10, 50 and 200 µm diameter particles injected from the same point at the inlet. It is well known that separation efficiency in a cyclone is governed by drag, centrifugal and gravitational forces. Swirling motion inside the cyclone cell causes the larger particles (10, 50 and 200 µm) to travel swiftly towards the wall due to the higher centrifugal forces finally escaping through the scavenging pipe. On the other hand the smaller particles (1 and 5µm) drift with the flow along the stream without being able to travel towards the wall andthese particles are carried away through the air outlet. From equations [3] and [4] it can be noted that for smaller particles drag dominates the centrifugal force where as for larger particles centrifugal force is high and the drag opposing the partcle motion is low, hence larger particles lag and have a tendency to drop down to the wall.

International Journal of Engineering Research & Technology (IJERT)
ISSN: 2278-0181
Vol. 5 Issue 08, August-2016

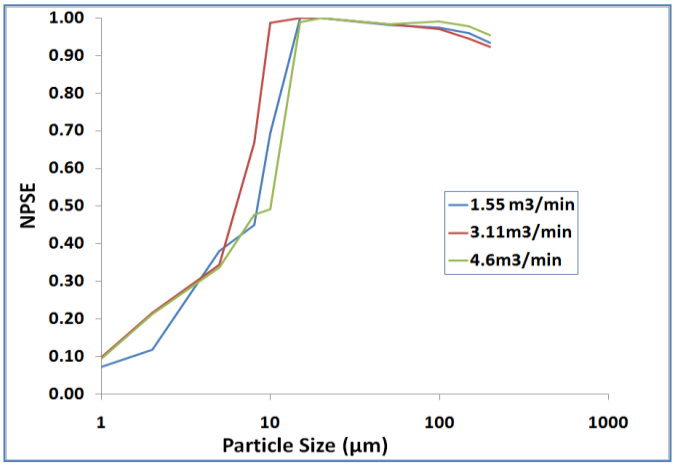


Figure 10: Plots of Normalized Separation Efficiency (%) Vs. Particle Size (µm) for 3 different flow rates including wall collision effects

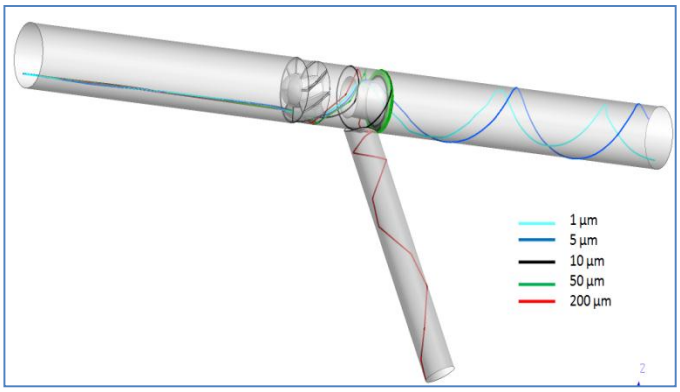


Figure 11: Particle tracks

*2. ISO 12103-1 Standard Distribution (Rosin-Rammler)*

The study of separation efficiency for homogeneous particle injection was followed by calculations for the Rosin-Rammler distribution with the ISO 12103-1 sample, both for with and without scavenging cases. These results, summarized in Table 5, are also obtained with default wall reflection coefficients (1,1). It can be observed that pre-separation efficiencies are not in fair agreement with experimental results and also CFD predicts decreasing separation efficiency with flow rate conflicting withthe experimental data where it increases with flow rate. While particle-particle collision effects have been ignored in the present study, it is reasonable to investigate the observed CFD behavior for different choice of wall reflection coefficients.The effect of the choice of wall reflection coefficients is investigated and reported in the next section.

Table 5: Pre-Separation Efficiency CFD Vs. Experimental

| Flow Rate ($m^3$/min) | Separation Efficiency (%) [With Scavenging] | | Separation Efficiency (%) [Without Scavenging] | |
|---|---|---|---|---|
| | Exp | CFD | Exp | CFD |
| 1.55 | 85.4 | 76.8 | 83.1 | 77.2 |
| 3.11 | 86.1 | 72.9 | 85.8 | 74.4 |
| 4.6 | -NA- | 70.7 | -NA- | - |
| 5.4 | -NA- | 70.8 | -NA- | - |

*C. Tuning of Reflection Co-efficient for Wall Collision Effects*

Dust particles experience loss of momentum when they collide with cyclone wall. Such loss of momentum is modeled by the wall reflection co-efficients(normal and tangential). Initial study of particle-wall collision is conducted on homogenous particles of six different sizes for two flow rates (1.55 and 3.11 $m^3$/min). The normal and tangential reflection co-efficients each is variedin steps of 0.25 keeping the other at the default value of 1.Variation of separation efficiency withreflection coefficient for different particle sizes is analyzed. The results of this analysis are presented in Figures 12 and 13 for two different flow rates. All the calculations are done by keeping 10% scavenging flow at dust outlet.

*1)Impact on Homogeneous Particles:*

*1.1) ForFlow Rate of1.55 $m^3$/min:*

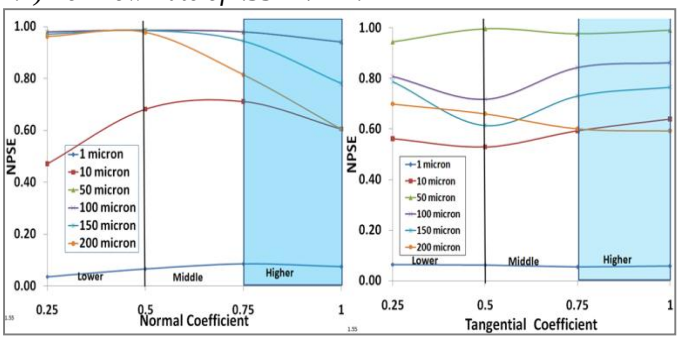


Figure 12: Impact of reflection coefficients on normalized separation efficiency for Individual homogeneous particle distribution

*1.2) For Flow Rate of 3.11 $m^3$/min:*

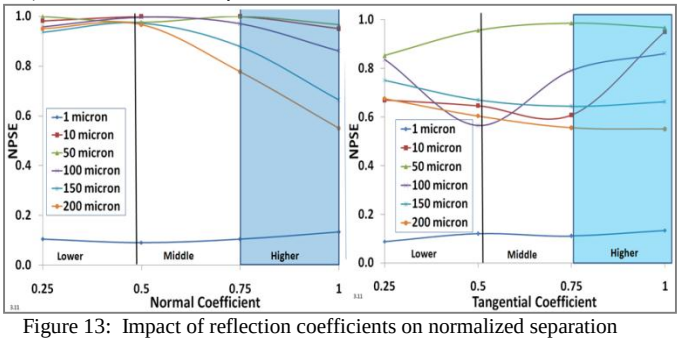


Figure 13: Impact of reflection coefficients on normalized separation efficiency for Individual homogeneous particle distribution

Figures 12 and 13,show that separation efficiency is more or less insensitive to reflection coefficients, (about 10%) in the case of smaller particles (1 and 10 µm). Separation efficiencies of larger particles however are seen to be sensitive to higher range of reflection coefficients that are generally associated with less loss of momentum. Wall collision effects especially in the region just downstream of the cyclone where the scavenging duct is located, may therefore need to be captured with certain amount of tuning of the reflection coefficients in preference to the default values. It is conceivable that the relative magnitudes of drag and gravity vis-a-vis particle size and the resulting trajectory may be more significantly affected by the choice of reflection coefficients in this region than elsewhere. The particle trajectories in Figure 9 seem to provide

International Journal of Engineering Research & Technology (IJERT)
ISSN: 2278-0181
Vol. 5 Issue 08, August-2016

corroborative evidence of this reasoning. Hence it was decided to investigate in detail the effect of wall reflection coefficients in the range 0.7 to 1 for the RR distribution. Figures 12 and 13 summarize the numerical results of this investigation in graphical plots.

*2)Impact on RR Distribution for Reflection coefficients between 0.7 and 1:*

*2.1) For Flow Rate of 1.55 $m^3$/min*

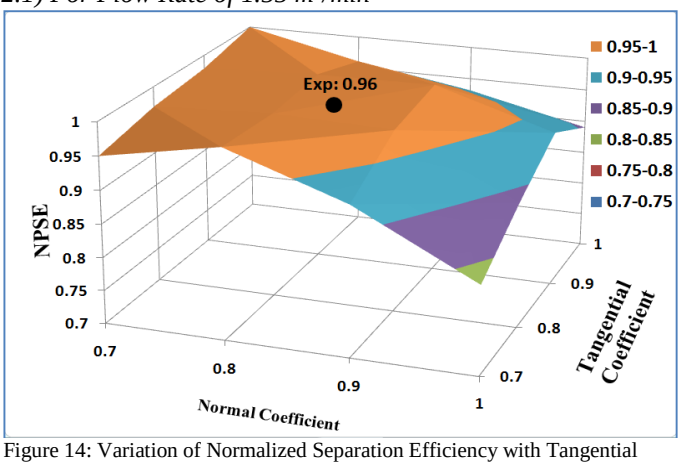


Figure 14: Variation of Normalized Separation Efficiency with Tangential and Normal co-efficient

*2.2) For Flow Rate of 3.11 $m^3$/min*

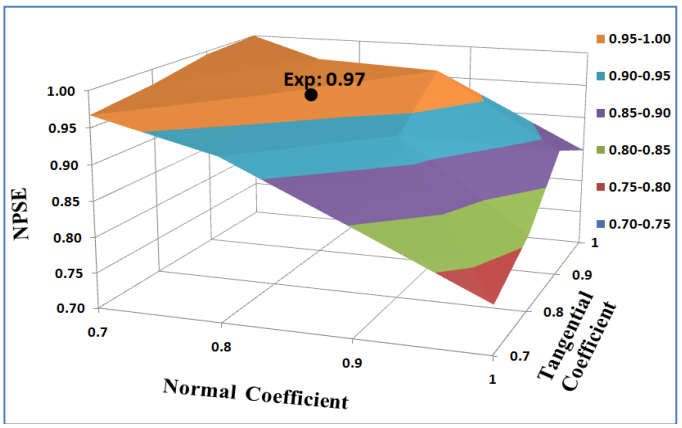


Figure 15: Variation of Normalized Separation Efficiency with Tangential and Normal co-efficient

Figure 14 and 15, show that accuracy of CFD prediction is close to experimental value 85.4 and 86.1(Normalized values 0.96 and 0.97) for flow rates 1.55 and 3.11 $m^3$/min respectivly when wall collision effects with some amount of momentum loss are included in the simulation.Recommended values of wall reflection coefficients [normal, tangential] are chosen on the basis of measured values of pre-separation efficiency. One can also observe that the trend of separation efficiency increasing with flow rate is recovered by the choice of the wall reflection coefficients.

## VI CONCLUSION

A CFD methodology based on flow simulation combined with Lagrangian particle tracking has been developed to calculate pressure drop and pre-separation efficiency for a single cyclone element. The present work shows that a hybrid meshing approach results in an optimal mesh for calculating flows through single cyclones and may be implemented in multi-cyclone geometries economically. The standard k-ε model with standard wall function appears to perform well with respect to the flows and dust loading conditions considered and the mesh employed. The discrete phase method (DPM) with Lagrangian particle tracking has been investigated for a relevant range of tangential and normal wall collision reflection coefficients. Based on comparison with experimental data, it is shown that an optimal choice of these coefficients may be arrived at, though the choice may need further corroboration over wider geometries, flow rates and dust loading. The DPM methodology with only the drag and gravity forces included, reveals that pre-separation efficiency can be calculated to within an error margin of about 6 % with measured data. Since turbulence dispersion effects have not been included in the present study, it is possible that inclusion of the same may influence the dispersion of the smaller particles of 10μm size or less and hence impact calculated pre-separation efficiency for a distribution of particles. Also the one-way coupling approach between flow and particle tracking adopted here seems to be adequate for the prediction of cyclone performance under conditions of small mass loading as used in the present study.

## ACKNOWLEDGEMENT

This project work has been carried out At the Crucible of Research and Innovation (CORI) of PES University with funding provided by Mann+Hummel Service center, Bengaluru, India as part of the industry-university collaboration program.

## REFERENCES

[1] M. Marinucand F. Rus , "The Effect Of Particle Size And Input Velocity On Cyclone Separation Process," Bulletin of the Transylvania University of Brasov, Vol. 4 (53) No. 2 - 2011.

[2] W. B. Faulkner and B. W. Shaw, "Efficiency And Pressure Drop Of Cyclones Across A Range Of Inlet Velocities," Applied Engineering in Agriculture ,ASABE, Vol. 22(1): 155-161, 2006.

[3] G. B. Sakura and Andrew Y. T. Leung, " Experimental Study of Particle Collection Efficiency of Cylindrical Inlet Type Cyclone Separator," IJESD, Vol. 6, No. 3, March 2015.

[4] L. Svarovsky, "Economics of gas cleaning; equipment selection," in Handbook of Powder Technology. vol. 3, J. C. Willams and T. Allen, Eds. Amsterdam: Elsevier Scientific Publishing Company, 1981.

[5] F. Zenz, "Cyclone separators," Manual on Disposal of Refinery Wastes; Volume on Atmospheric Emissions, API Publications, 1975.

[6] E. Muschelknautz, "Die berechnung von zyklonabscheidernfürgase,"*ChemieIngenieurTechnik*, vol. 44, pp. 63-71, 1972.

[7] E. Muschelknautz and W. Krambrock, "Design of cyclone separators in the engineering practice," *Staub-Reinhalt. Luft*, vol. 30, pp. 1-12, 1970.

[8] Jolius Gimbun, Thomas S Y , et al, "A CFD Study On Prediction of Cyclone Collection Efficiency,"IJCMES, July 2005.

[9] Francisco José de Souza, Ricardo de VasconcelosSalvo, et al, "Large Eddy Simulation of The Gas Particle Flow In a Cyclone Separator," Separation and Purification Technology 94, 31-70, 2012.

[10] Hemdan Shalaby, Klaus Wozniak et al," Numerical Calculation of Particle-Laden Cyclone Separator Flow Using LES," Engineering Applications of Computational Fluid Mechanics, 2:4, 382-392,2008.

[11] M Sommerfeld "Analysis of Collision Effects for Turbulent Gas-Particle Flow in a Horizontal Channel: Part I. Particle Transport" International Journal of Multiphase Flow 29 675-699, 2003.

[12] ANSYS FLUENT User Guide, Modeling Multiphase Phase Flows.